

Vascular segmentation of neuroimages based on a prior shape and local statistics^{*}

Yun TIAN^{1,2}, Zi-feng LIU^{1,2}, Shi-feng ZHAO^{†‡1,2}

¹College of Information Science and Technology, Beijing Normal University, Beijing 100875, China

²Beijing Key Laboratory of Digital Preservation and Virtual Reality for Cultural Heritage, Beijing 100875, China

[†]E-mail: zhao_shifeng@bnu.edu.cn

Received Mar. 2, 2018; Revision accepted July 31, 2018; Crosschecked Aug. 15, 2019

Abstract: Fast and accurate extraction of vascular structures from medical images is fundamental for many clinical procedures. However, most of the vessel segmentation techniques ignore the existence of the isolated and redundant points in the segmentation results. In this study, we propose a vascular segmentation method based on a prior shape and local statistics. It could efficiently eliminate outliers and accurately segment thick and thin vessels. First, an improved vesselness filter is defined. This quantifies the likelihood of each voxel belonging to a bright tubular-shaped structure. A matching and connection process is then performed to obtain a blood-vessel mask. Finally, the region-growing method based on local statistics is implemented on the vessel mask to obtain the whole vascular tree without outliers. Experiments and comparisons with Frangi's and Yang's models on real magnetic-resonance-angiography images demonstrate that the proposed method can remove outliers while preserving the connectivity of vessel branches.

Key words: Vesselness filter; Neighborhood; Blood-vessel segmentation; Outlier

<https://doi.org/10.1631/FITEE.1800129>

CLC number: TP391.4

1 Introduction

Vascular segmentation is an important method in the quantification of morphological changes of blood vessels, enabling an accurate diagnosis during treatment processes (Forkert et al., 2013). For example, brain stroke, which is often caused by stenosis of cerebral vessels, is the third most common cause of death and a major cause of long-term disabilities. It is important to investigate initial symptoms at an early stage with the aim of eliminating the need for invasive treatments (Chowriappa et al., 2013). Therefore, the accuracy and visualization of the extracted vessels

become key factors. However, it is difficult to accurately extract blood vessels because of the high complexity of cerebrovascular anatomical structures, limited spatial resolution, and low image contrast of medical images, such as magnetic-resonance-angiography (MRA) images (Bogunović et al., 2011).

For vascular segmentation, a large number of algorithms have been developed, including the semi-automatic and automatic segmentation. As manual segmentation is subjective and prone to human errors, automatic approaches are commonly used. One of the well-known techniques is the active contour model, based on the geometric curve evolutionary theory (Zhao et al, 2014; Chen et al., 2018); it has facilitated the accurate extraction of neuroimages (Wang et al., 2015; Woźniak and Strzelecki, 2015). Active contour models are usually implemented by a level-set framework by locally minimizing an energy function with a gradient-descent algorithm (Ding et al., 2014). The statistics-based method has been another typical

[‡] Corresponding author

^{*} Project supported by the National Natural Science Foundation of China (Nos. 61472042 and 61802020), the Beijing Natural Science Foundation, China (No. 4174094), and the Fundamental Research Funds for the Central Universities, China (No. 2015KJJC25)

 ORCID: Shi-feng ZHAO, <http://orcid.org/0000-0002-5037-169X>
© Zhejiang University and Springer-Verlag GmbH Germany, part of Springer Nature 2019

choice for vessel segmentation (El-Baz et al., 2012; Tian et al., 2013). The finite mixture model has been widely used to assign each pixel to a finite number of classes according to the statistical properties of the pixels and its neighbors (Adel et al., 2010). The expectation-maximization (EM) algorithm is often employed to estimate the unknown parameters.

In addition, the enhancement filter proposed by Frangi et al. (1998), which analyzes the second-order derivatives encoded in the Hessian matrix, has been frequently used. Vessels with various widths can be depicted by determining the vesselness of the image at multiple scales (Kumar et al., 2015). Yang et al. (2012) proposed an improved Frangi method for the preprocessing of coronary artery segmentation by adding geometric information obtained from ray-casting in a local sphere, for discriminating tubular structure between false step-edge responses at the heart chamber and positive vessel responses. Becker et al. (2013) proposed a vesselness-based method for the tracing of vessel trees. Rajeswari and Jagannath (2017) proposed an enhancement filter based on the ratio of multi-scale eigenvalues of the Hessian matrix. Such vesselness information for the quantification of the likelihood of each voxel belonging to a vascular or non-vascular structure can be employed for initialization of other methods, such as the Canny refinement algorithm (Yang X et al., 2014) and the local entropy approach (Hibet-Allah et al., 2016).

However, the results of the above methods may not be satisfactory because of the existence of outliers, which obscure the blood vessels. The outliers may emerge from real thin vessels or non-vessel structures such as subcutaneous fat, with high intensities because of the intensity overlap between them. They exist in the form of small islands; thus, it is necessary to remove them. To the best of our knowledge, this problem has not been investigated in detail.

A common dilemma is that when more vessels are segmented, more outliers can be produced. As the outlier voxels have similar intensities with the vessels, the simple thresholding method cannot analyze them. The connectivity filter (the largest-connected-component approach) is the most frequently employed method to remove outliers. This method selects the largest (few) connected vascular tree(s) using a three-dimensional-region-growing algorithm (El-Baz et al., 2005). However, most researchers have men-

tioned it as only a post-processing procedure without detailed discussion (Chan et al., 2006; Sulayman et al., 2016). In addition, some fractions at the tails of vessels and isolated small branches may be missing.

To address the above challenges, in this study, we present a novel method for the refinement of blood-vessel segmentation. First, a vesselness mask, based on the vascular shape characteristic, is defined. It quantifies the likelihood of each voxel belonging to a bright tubular-shaped structure. Two operations, including connection component selection and vascular structure refinement, are then employed to extract the blood vessels.

2 Related work

As the intensities of some surrounding tissues such as the brain tissue are very close to those of blood vessels, there are some non-vessel voxels, i.e., outlier points, in the segmentation results. To effectively remove outlier points emerging around the vessels, shape (geometric) features of the vessels need to be considered. Using all of the eigenvalues of the Hessian matrix, some vesselness filters can fully consider geometric features represented by the eigenvalues and suppress the noise impacts on vessels. In this section, two related studies are discussed.

2.1 Frangi's model

Frangi's model, based on vesselness, is a well-known and extensively used method to enhance tubular structures. It maps each pixel to a real number between 0 and 1, which represents to which extent the pixel belongs to a tubular structure.

The vessel shape can be represented by an eigenanalysis of the Hessian matrix \mathbf{H} of a dataset. The Hessian matrix is a square matrix of second-order partial derivatives of a function; it can be used to describe the local intensity variation of an image. The Hessian matrix for a three-dimensional (3D) image $I(\mathbf{x})$ ($\mathbf{x}=(x, y, z)$) can be expressed as

$$\mathbf{H} = \nabla^2 I(\mathbf{x}) = \begin{bmatrix} I_{xx}(\mathbf{x}) & I_{xy}(\mathbf{x}) & I_{xz}(\mathbf{x}) \\ I_{yx}(\mathbf{x}) & I_{yy}(\mathbf{x}) & I_{yz}(\mathbf{x}) \\ I_{zx}(\mathbf{x}) & I_{zy}(\mathbf{x}) & I_{zz}(\mathbf{x}) \end{bmatrix}, \quad (1)$$

where the second-order partial derivatives can be obtained by the convolution of $I(\mathbf{x})$, and the second-order partial derivative of the Gaussian function $G(\mathbf{x}; \sigma_f)$ with a variance of σ_f is $I_{xx}(\mathbf{x}) = \{\partial^2 G(\mathbf{x}; \sigma_f) / \partial x^2\} \cdot I(\mathbf{x})$. Denote the eigenvalue with the k^{th} smallest magnitude ($|\lambda_1| \leq |\lambda_2| \leq |\lambda_3|$) as λ_k ; the corresponding eigenvectors correspond to a singular direction. The geometric meaning of these eigenvectors at point \mathbf{x} in the vessel region is described in Fig. 1.

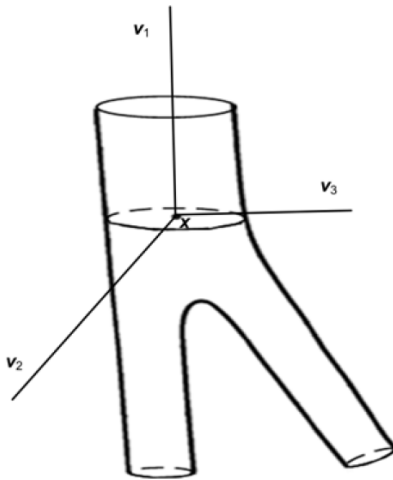


Fig. 1 Geometric meaning of the eigenvectors v_1 , v_2 , and v_3 of the Hessian matrix H at point \mathbf{x} in the vessel region
 v_1 indicates the direction along the vessel (the minimum intensity variation), and v_2 and v_3 form a basis for the orthogonal plane

Regarding bright vessels with a dark background in MRA and computed-tomography-angiography (CTA) images, an ideal tubular structure should satisfy the following relationship:

$$|\lambda_1| \approx 0, |\lambda_1| \leq |\lambda_2|, \lambda_2 \approx \lambda_3. \quad (2)$$

Three geometric ratios R_A , R_B , and S are defined as

$$\begin{cases} R_A = \frac{|\lambda_1|}{\sqrt{|\lambda_2 \lambda_3|}}, \\ R_B = \frac{|\lambda_2|}{|\lambda_3|}, \\ S = \sqrt{\lambda_1^2 + \lambda_2^2 + \lambda_3^2}, \end{cases} \quad (3)$$

where R_A differentiates the plane structures from the line structures in the latter case where its value is zero, R_B is the maximum for a blob structure, and S is a

measure to distinguish a low-intensity background as the eigenvalues are small in the background. Based on these three parameters, a vesselness measure $V_\sigma(S)$ can be expressed as

$$V_\sigma(S) = \begin{cases} 0, & \lambda_2 > 0 \text{ or } \lambda_3 > 0, \\ (1 - e^{-R_A^2 / (2\alpha^2)}) \cdot e^{-R_B^2 / (2\beta^2)} \cdot (1 - e^{-S^2 / (2\gamma^2)}), & \text{otherwise,} \end{cases} \quad (4)$$

where α , β , and γ are thresholds of the 3D vesselness function used to control the sensitivity of the vessel enhancement filter to the parameters of R_A , R_B , and S . The multiscale theory is applied to the vesselness measure because of the different sizes of blood vessels. The vesselness function of Eq. (4) has the maximum response in the case where the spatial scale factor σ is approximately equal to the practical size of the vessels. Therefore, the vesselness measure corresponding to several scale factors of each voxel can be calculated; the maximum response value is obtained by

$$R(S) = \max_{\sigma_{\min} \leq \sigma \leq \sigma_{\max}} \{R_\sigma(S)\}, \quad (5)$$

where σ_{\min} and σ_{\max} denote the minimum and maximum scales, respectively. In this model, the boundary of a non-vessel structure with the same intensity as the vessels can cause a step-edge response, which can easily lead to a false segmentation result (Yang et al., 2012). In addition, it cannot properly enhance vessels throughout crossings or bifurcations corresponding to a large part of the vascular network (Hannink et al., 2014).

2.2 Yang's model

With the enhancement of vascular structures, other tubular structures such as nasal soft tissue in the brain MRA images are simultaneously enhanced in Frangi's model, which certainly increases the segmentation difficulty of blood vessels. The Hessian multiscale measure in Eq. (4) considers only the local geometric features without the global gray-scale information; consequently, some pseudo blood vessels and many isolated outliers emerge in the enhancement results. To resolve this issue, Yang JZ et al. (2014) proposed an improved method based on Frangi's

model. An image gray-scale factor F is added to the vesselness function, expressed as

$$V_{\sigma}(S) = \begin{cases} 0, & \lambda_2 > 0 \text{ or } \lambda_3 > 0, \\ \left(1 - e^{-R_A^2/(2\alpha^2)}\right) \cdot e^{-R_B^2/(2\beta^2)} \cdot \left(1 - e^{-S^2/(2\gamma^2)}\right) \cdot F, & \text{otherwise.} \end{cases} \quad (6)$$

Specifically, we have

$$F = \frac{1}{2} \left[1 + \frac{2}{\pi} \arctan \left(\frac{I(\mathbf{x}) - \text{Hu}}{P_{\max}} c \right) \right], \quad (7)$$

where P_{\max} is the maximum gray value of the images and c the smoothness factor of F . Fig. 2 shows the graph of F when $c=1$.

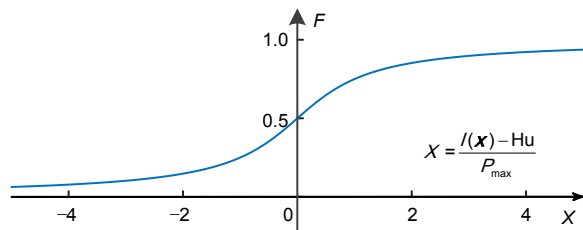


Fig. 2 Graph of F defined in Eq. (7) when $c=1$

The parameter of Hu in Eq. (7) is computed by employing an iterative threshold method. It calculates the average image gray value, and is used to roughly segment the original image into foreground and background. The process is repeated until the threshold does not change; it is implemented by a mathematical expression as

$$T_{i+1} = \frac{1}{2} \left(\frac{\sum_{k=1}^{T_i} h_k \cdot k}{\sum_{k=1}^{T_i} h_k} + \frac{\sum_{k=T_i+1}^{L-1} h_k \cdot k}{\sum_{k=T_i+1}^{L-1} h_k} \right), \quad (8)$$

where L is the number of gray scales and h_k the number of voxels with a gray value of k . The iteration is repeated until T_i is equal to T_{i+1} , leading to the final segmentation threshold, i.e., $\text{Hu}=T_i$.

According to the curve of F shown in Fig. 2, the voxels whose gray values are larger than Hu can be enhanced further, while the voxels whose gray values

are smaller than Hu will be suppressed. Therefore, the pseudo vessel structures and isolated outliers may be removed. However, the model still has the common drawback that other threshold-based methods share; i.e., the vessels with intensities lower than the threshold are suppressed, meaning that there is a requirement to determine an accurate threshold.

3 The proposed methodology

3.1 Vesselness filter definition

Inspired by Frangi’s and Yang’s models, a vesselness filter is defined. The vesselness value is a real number between 0 and 1. If a voxel belongs to a tubular-like structure, the corresponding vesselness value is close to 1; otherwise, it is close to 0. In Frangi’s and Yang’s models, the object shape is judged on the basis that for an ideal tubular structure, $R_B \approx 0$ and $R_A \approx 1$; for an ideal plate-like structure, $R_B \approx 0$ and $R_A \approx 0$ (this explains the inability to differentiate a plate-like structure from a tubular structure by only R_B); for an ideal blob-like structure, $R_B \approx 1$ and $R_A \approx 1$. The relationship between the shape and the corresponding eigenvectors is illustrated in Fig. 3.

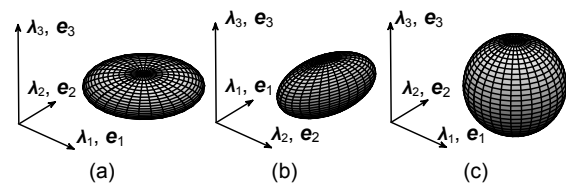


Fig. 3 Isosurface representations of the structures and the corresponding eigenvalues: (a) plate-like; (b) tubular-like; (c) blob-like

Note that if $R_B \approx 0$, the second term in the second line of Eq. (6) is close to 1; however, if $R_A \approx 1$, the first term in the second line of Eq. (6) is not sufficiently close to 1, represented by the red lines in Fig. 4. Therefore, to efficiently enhance the tubular structure, a novel vesselness filter is defined in Eq. (9), which is expressed at the top of the next page.

The defined function in Eq. (9) can provide a strong response of the filter at tubular voxels (blue curves in Fig. 4). This function may almost simultaneously enhance the other two shape structures; however, this is not very important in the presented methodology as the enhancement result is intended to

$$V_{\sigma}(S) = \begin{cases} 0, & \lambda_2 > 0 \text{ or } \lambda_3 > 0, \\ \left\{ 1 - \exp\left[-\frac{\tan^2\left(\frac{\pi}{2} \cdot R_A\right)}{2\alpha^2}\right] \right\} \cdot \exp\left[-\frac{\tan^2\left(\frac{\pi}{2} \cdot R_B\right)}{2\beta^2}\right] \cdot \left[1 - \exp\left(-\frac{S^2}{2\gamma^2}\right) \right] \cdot F, & \text{otherwise.} \end{cases} \quad (9)$$

be further processed to become a mask. This requires retention of more details of the blood vessels. In addition, the adaptive method proposed in Eq. (8) improves the algorithm performance. The threshold of Hu evaluated by Yang’s model is too low to suppress non-vessel issues. An example of the distribution of gray values of a brain MRA dataset is shown in Fig. 5.

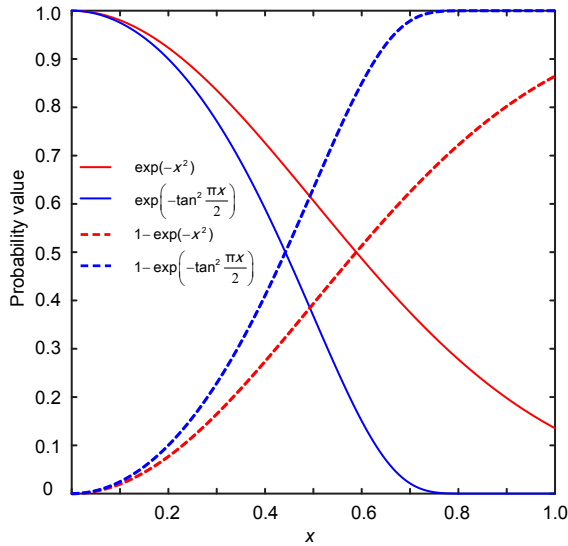


Fig. 4 Comparison between the first two terms in the original vesselness function (red curves) and those of the proposed method (blue curves)

Solid curves represent the second term which includes R_B , while dotted curves represent the first term which includes R_A . References to color refer to the online version of this figure

For the brain MRA images, the gray values are in the range of 0 to more than 1100; over 95% of the voxels have gray values smaller than 300 (the other 5% are mainly vessels). According to the proposed adaptive threshold method in Eq. (8), initially, the global average gray value T_0 should be calculated. The histogram of the volume data usually shows two peaks (Fig. 5). The value of the lowest point between the two peaks is chosen as the initial value of T_0 . In the example shown in Fig. 5, this value is 85, which divides the original image into foreground and background. The mean gray value of the foreground,

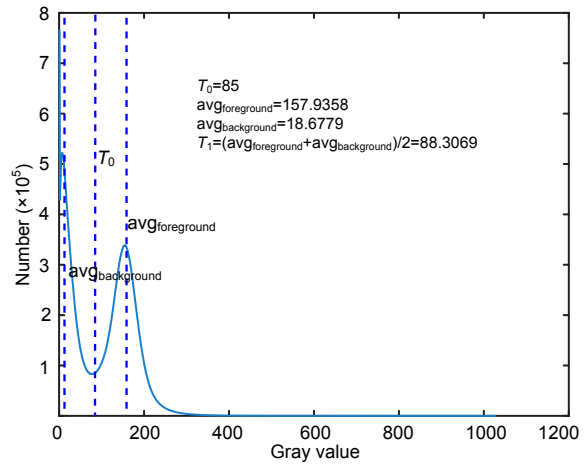


Fig. 5 Gray histogram of a brain MRA dataset

Two peaks are observed, representing the background and foreground. A long tail in a high-intensity region (approximately 300–1000) after the rightmost peak is observed, which indicates the cerebral vessels

denoted as $avg_{\text{foreground}}$ in Fig. 5, and mean gray value of the background, denoted as $avg_{\text{background}}$ in Fig. 5, are then calculated.

3.2 Connection component selection

After filtering the blood vessels, a branch-connecting operation is implemented. For the voxels of the blood vessels, 26-neighbor connection components (CCs) are all searched by the vesselness filter, and denoted with the numbers from 1 to m . Considering that vessels are structures with high vesselness values, consisting of a large number of voxels, these voxels can be sorted using a parameter C_i , defined as

$$C_i = w_1 N_i + w_2 A_i, \quad (10)$$

where N_i is the normalized number of voxels in the i^{th} CC, A_i the normalized average gray value (the gray value here is the rescaled vesselness value in the range of 0 to 255, instead of the original gray value) of the voxels in the i^{th} CC, and w_1 and w_2 the weights of each part. The case where $w_1=1$ and $w_2=0$ corresponds to the general connectivity filter method.

In the implementation, we adjust w_1 and w_2 , and obtain the dice coefficient of the segmentation result in Fig. 6 (preserving 20 CCs). We set $w_1=0.2$ and $w_2=0.8$ for each dataset. After sorting all C_i values of the m CCs, the top k ($k < m$) CCs are preserved. Thus, some small isolated issues are removed. A mask with main tubular structures and rough segmentation of blood vessels is obtained, and can be used to remove outliers in the segmentation procedure.

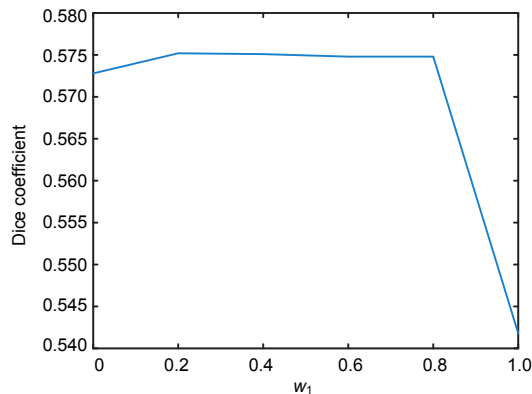


Fig. 6 Segmentation results for different weights

3.3 Vascular structure refinement

Denote the segmentation volume as V_s and the mask volume as V_m . The refinement procedure is implemented based on a region-growing method; the pseudo-code is presented in Algorithm 1.

Algorithm 1 Refinement of segmentation

```

1: function Refinement of segmentation
2:    $F \leftarrow 0$  //  $F$  is of the same size as  $V_s$ 
3:   for each non-background voxel  $V_s(i, j, k)$  in  $V_s$  do
4:     if the corresponding voxel  $V_m(i, j, k)$  is non-
       background and  $F(i, j, k)=0$  then
5:        $F(i, j, k) \leftarrow 1$ 
6:       RegionGrowing( $V_s, F, i, j, k$ )
7:     end if
8:   end for
9:   for each non-background voxel  $V_m(i, j, k)$  in  $V_m$  do
10:    if  $F(i, j, k)=1$  then
11:      set  $V(i, j, k)$  to be background
12:      // keep only the region-growing result
13:    end if
14:   end for
15:   return  $V_s$ 
end function

```

The function RegionGrowing involves V_s and F as arguments. For each input voxel $V_s(i, j, k)$, it

expands to its 26-neighbor non-background voxels with depth-first search. For the newly expanded region, F is set to one. After the application of this RemoveNoise function, isolated outliers are removed while disconnected far ends of the small vessels are kept (as long as the vessels appear in the mask). The complete procedure is illustrated in Fig. 7.

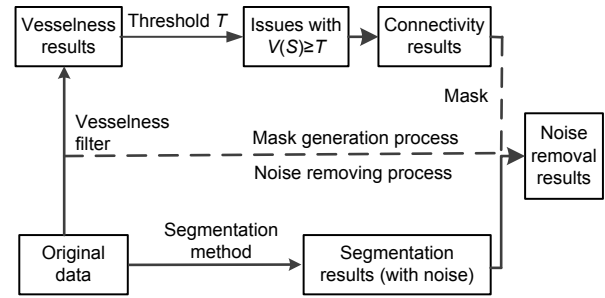


Fig. 7 Flowchart of the proposed method

4 Results and discussion

In the experiments, several 3D MRA brain datasets were employed to evaluate the proposed method. Implementation details and experimental results are presented.

4.1 Blood vessel mask

As the intensities of some tissues are close to those of vessel structures, some non-blood vessel points often exist in the segmentation results. First, the proposed vesselness filter and connection selection were applied to the original image. However, this did not completely and effectively segment the blood vessels because of some outliers with tubular shapes.

To illustrate the gray values of the vascular structures, we employed a threshold process (Eq. (8)) on an original MRA brain image, where voxels with gray values lower than H_u were set to zero. Table 1 presents the ratio of the remaining structures to the whole brain, while Fig. 8 shows the remaining parts after the threshold process, for different values of H_u .

The term F added in Eq. (9) suppresses the non-vessel structures with tubular shapes, particularly nasal structures in the MRA brain images. As H_u was used as a threshold in F , it should be properly set to achieve a balance, where the effect of the intensity overlap between vessels and outliers can be reduced. To preserve as many small vessels (with low

intensities) as possible, Hu should be relatively low. In this study, Hu was set to 200. Fig. 9 shows that the distribution of the voxel number to intensity is similar to a normal distribution with a mean value of 200. A blood vessel mask was then generated through global thresholding.

Table 1 Different thresholds of Hu and volume ratios of the preserved parts

Threshold of Hu	Volume ratio (%)
100	54.2912
150	32.2688
200	6.1140
250	1.3543
300	0.4750
350	0.2179

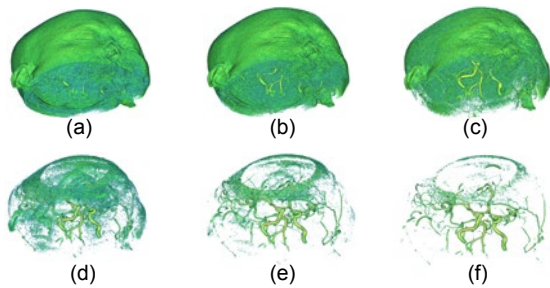


Fig. 8 Blood vessel mask with different thresholds of Hu: (a) Hu=100; (b) Hu=150; (c) Hu=200; (d) Hu=250; (e) Hu=300; (f) Hu=350

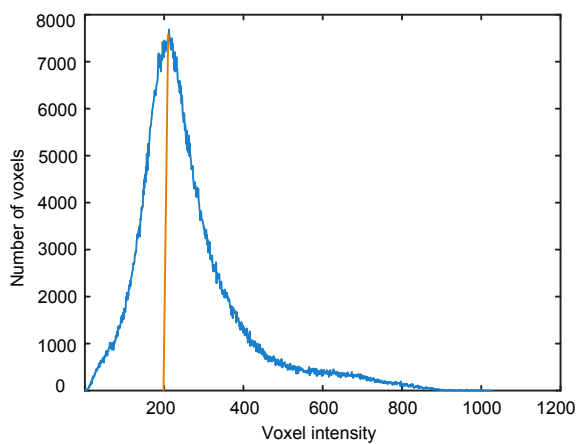


Fig. 9 Distribution of the preserved voxels after vesselness

4.2 Outlier removal

The difference between the proposed region-growing method and the traditional method is that the average gray value of the images is considered in our method. The average gray value of a CC was

important for the final accurate segmentation, as there existed some isolated small vessels that need to be retained, and some large components such as nasal structures that need to be removed. The weight w_2 should be larger when fewer CCs were preserved; we set $w_2=0.8$ in the experiments. In addition, it was important to keep an appropriate number of components; we set $k=15$.

The first row of Fig. 10 shows the outlier removal results from cerebral vessels of an MRA dataset, initially segmented by the active contour model, obtained with different methods, including Frangi's, Yang's, and our models. The second row of Fig. 10 shows the amplified spatial details corresponding to the local region marked with a box in the first row. The first column of Fig. 10 shows that some outliers disrupt the blood vessels segmented by the method without shape information. The second column of Fig. 10 shows that Frangi's model can remove most of the outliers, even some small blood vessels are eliminated, as the boundary of a non-vessel structure with the same intensity as that of a vessel has a high edge response. The third column of Fig. 10 shows that Yang's model can extract most of the vessels; however, some blood vessels at the bifurcation are missed, as an inappropriate threshold is employed and the vessels with intensities lower than the threshold are suppressed. It is challenging to determine an accurate threshold. The last column of Fig. 10 shows that our model can accurately extract thick and thin vessels. Furthermore, the extracted cerebral tree is observed with a good connectivity. The excellent performance of our method is attributed to the use of neighborhood statistics.

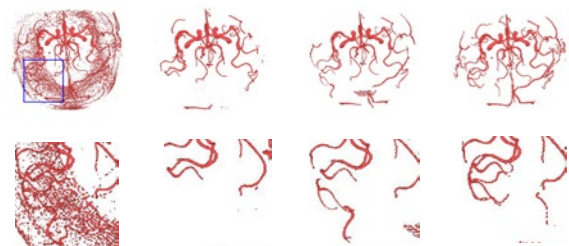


Fig. 10 Comparison of our method with Frangi's and Yang's models

Column 1 shows the segmentation results of the cerebral vessels by the active contour model; columns 2–4 show the outlier removal results from the cerebral vessels of Frangi's, Yang's, and our models, respectively. Enlarged views of the spatial location marked with a box for the different models are shown in the second row

In addition, three MRA brain datasets were employed to validate the proposed model. Fig. 11 shows the segmentation results for the three MRA datasets, obtained with different methods including Frangi's, Yang's, and our models. Each row of Fig. 11 corresponds to one of the datasets. The first column of Fig. 11 shows that the vessel masks were extracted using the proposed filter. These vessel masks contained the whole cerebral tree and outliers. Outlier removal was then applied to the segmented mask with Frangi's, Yang's, and our models; the results are shown in columns 2–4 in Fig. 11.

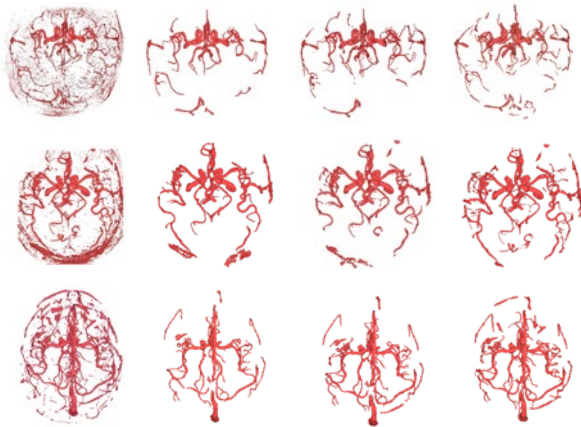


Fig. 11 Comparison of our method with Frangi's and Yang's models on three MRA brain datasets

Column 1 shows the results of the original Frangi vesselness filter; columns 2–4 show the outlier removal results from the cerebral vessels with Frangi's, Yang's, and our models, respectively. The results of the different datasets are presented in different rows

These results demonstrate that our method can distinguish all outliers and blood vessels, as the tangent term is added to the vesselness filter defined in Eq. (9); the addition of the F term (Eq. (7)) to the model enables the suppression of the non-vessel-shape structure issues, such as the nasal structure. If the brain has undergone skull-stripping, it is not necessary to use it in Eq. (7). Furthermore, note that the thin branches disconnected from the thick vessel were extracted in the segmentation results obtained by our model.

4.3 Performance evaluation

We investigated aspects of performance evaluation such as the quality of segmentation and the computational time. We compared Frangi's, Yang's,

and our methods in terms of sensitivity, specificity, and the dice similarity coefficient (DSC). The average performance measures are shown in Table 2, which reveals that the proposed model provides better sensitivity and DSC scores than the other two methods. Note that our method has a similar specificity performance to Frangi's and Yang's models.

Table 2 Performances of the three methods

Method	Sensitivity	Specificity	DSC
Frangi's	0.602 74	0.978 29	0.647 06
Yang's	0.704 76	0.983 87	0.751 27
Ours	0.782 61	0.986 58	0.850 39

DSC: dice similarity coefficient

The computational time was evaluated. We randomly selected nine datasets for evaluation. Datasets 1–3 were acquired from the Beijing Tiantan Hospital, datasets 4–6 were acquired from the Navy General Hospital, and datasets 7–9 were obtained from a publicly available MIDAS (<http://insight-journal.org/midas/>) dataset. Table 3 shows the corresponding computational time. The experiments were implemented in Matlab 2014b, and run on a PC with Intel Core i5, 3.3 GHz CPU, and 12 GB RAM. We considered only the running time of the filtering procedure, where differences existed among the three methods. Table 3 reveals that the proposed method does not increase the computational complexity upon the addition of other equations.

5 Conclusions

We have presented a novel method for segmentation of blood vessels from MRA datasets. The entire vessel tree could be extracted by our method, which uses neighborhood statistics and shape information. First, a vesselness filter with a strong response at tubular voxels has been defined, and an analysis of the CCs has been performed to obtain a blood-vessel mask containing thick and thin vessels and some outliers. A region-growing method based on local statistics has been implemented on the vessel mask to obtain the whole vascular tree without outliers. The results showed that our efficient and robust model could accurately extract the entire cerebral tree. Furthermore, the proposed method can be used for

Table 3 Comparison of computational costs of the three methods

Dataset	Data size (pixel)	Spatial resolution (mm×mm×mm)	Computational time (min)		
			Frangi's method	Yang's method	Proposed method
1	512×512×136	0.39×0.39×1.2	4.23	4.25	4.49
2	512×512×136	0.39×0.39×1.2	4.19	4.20	4.20
3	512×512×117	0.39×0.39×1.2	3.36	3.49	3.49
4	512×512×216	0.47×0.47×1.4	7.03	7.42	7.07
5	512×512×216	0.47×0.47×1.4	6.40	6.41	6.43
6	512×512×176	0.47×0.47×1.4	5.48	5.50	5.51
7	448×448×128	0.50×0.50×0.8	2.46	2.48	2.49
8	448×448×128	0.50×0.50×0.8	2.47	2.49	2.50
9	448×448×128	0.50×0.50×0.8	2.47	2.48	2.50

extraction of the coronary artery, which has a similar tubular structure to the brain blood vessels. The proposed model could be further developed, for example, by including a procedure to efficiently determine the threshold of Hu.

Compliance with ethics guidelines

Yun TIAN, Zi-feng LIU, and Shi-feng ZHAO declare that they have no conflict of interest.

References

- Adel M, Moussaoui A, Rassigni M, et al., 2010. Statistical-based tracking technique for linear structures detection: application to vessel segmentation in medical images. *IEEE Signal Process Lett*, 17(6):555-558. <https://doi.org/10.1109/LSP.2010.2046697>
- Becker C, Rigamonti R, Lepetit V, et al., 2013. Supervised feature learning for curvilinear structure segmentation. Int Conf on Medical Image Computing and Computer-Assisted Intervention, p.526-533. https://doi.org/10.1007/978-3-642-40811-3_66
- Bogunović H, Pozo JM, Villa-Uriol MC, et al., 2011. Automated segmentation of cerebral vasculature with aneurysms in 3DRA and TOF-MRA using geodesic active regions: an evaluation study. *Med Phys*, 38(1):210-222. <https://doi.org/10.1118/1.3515749>
- Chan MY, Wu YC, Qu HM, et al., 2006. MIP-guided vascular image visualization with multi-dimensional transfer function. 24th Computer Graphics Int Conf, p.372-384. https://doi.org/10.1007/11784203_32
- Chen L, Mossa-Basha M, Balu N, et al., 2018. Development of a quantitative intracranial vascular features extraction tool on 3DMRA using semiautomated open-curve active contour vessel tracing. *Magn Reson Med*, 79(6):3229-3238. <https://doi.org/10.1002/mrm.26961>
- Chowriappa A, Kesavadas T, Mokin M, et al., 2013. Vascular decomposition using weighted approximate convex decomposition. *Int J Comput Assist Radiol Surg*, 8(2):207-219. <https://doi.org/10.1007/s11548-012-0766-6>
- Ding Y, Ward WOC, Wästerlid T, et al., 2014. Three-dimensional vessel segmentation using a novel combinatory filter framework. *Phys Med Biol*, 59(22):7013-7029. <https://doi.org/10.1088/0031-9155/59/22/7013>
- El-Baz A, Farag AA, Gimel'farb G, et al., 2005. Automatic cerebrovascular segmentation by accurate probabilistic modeling of TOF-MRA images. Int Conf on Medical Image Computing and Computer-Assisted Intervention, p.34-42. https://doi.org/10.1007/11566465_5
- El-Baz A, Elnakib A, Khalifa F, et al., 2012. Precise segmentation of 3-D magnetic resonance angiography. *IEEE Trans Biomed Eng*, 59(7):2019-2029. <https://doi.org/10.1109/TBME.2012.2196434>
- Forkert ND, Schmidt-Richberg A, Fiehler J, et al., 2013. 3D cerebrovascular segmentation combining fuzzy vessel enhancement and level-sets with anisotropic energy weights. *Magn Reson Imag*, 31(2):262-271. <https://doi.org/10.1016/j.mri.2012.07.008>
- Frangi AF, Niessen WJ, Vincken KL, et al., 1998. Multiscale vessel enhancement filtering. 1st Int Conf on Medical Image Computing and Computer-Assisted Intervention, p.130-137. <https://doi.org/10.1007/BFb0056195>
- Hannink J, Duits R, Bekkers E, 2014. Vesselness via multiple scale orientation scores. <https://arxiv.org/abs/1402.4963>
- Hibet-Allah O, Hajer J, Kamel H, 2016. Vascular tree segmentation in MRA images using Hessian-based multiscale filtering and local entropy thresholding. 2nd Int Conf on Advanced Technologies for Signal and Image Processing, p.325-329. <https://doi.org/10.1109/ATSIP.2016.7523100>
- Kumar RP, Albrechtsen F, Reimers M, et al., 2015. Blood vessel segmentation and centerline tracking using local structure analysis. 6th European Conf of the Int Federation for Medical and Biological Engineering, p.122-125. https://doi.org/10.1007/978-3-319-11128-5_31
- Rajeswari J, Jagannath M, 2017. Advances in biomedical signal and image processing—a systematic review. *Inform Med Unlocked*, 8:13-19. <https://doi.org/10.1016/j.imu.2017.04.002>
- Sulayman N, Al-Mawaldi M, Kanafani Q, 2016. Semi-automatic detection and segmentation algorithm of sac-

- cular aneurysms in 2D cerebral DSA images. *Egypt J Radiol Nucl Med*, 47(3):859-865.
<https://doi.org/10.1016/j.ejrm.2016.03.016>
- Tian Y, Duan FQ, Lu K, et al., 2013. A flexible 3D cerebrovascular extraction from TOF-MRA images. *Neuro-computing*, 121:392-400.
<https://doi.org/10.1016/j.neucom.2013.05.031>
- Wang R, Li C, Wang J, et al., 2015. Threshold segmentation algorithm for automatic extraction of cerebral vessels from brain magnetic resonance angiography images. *J Neurosci Methods*, 241:30-36.
<https://doi.org/10.1016/j.jneumeth.2014.12.003>
- Woźniak T, Strzelecki M, 2015. Segmentation of 3D magnetic resonance brain vessel images based on level set approaches. *Signal Processing: Algorithms, Architectures, Arrangements, and Applications*, p.56-61.
<https://doi.org/10.1109/SPA.2015.7365133>
- Yang GY, Kitslaar P, Frenay M, et al., 2012. Automatic centerline extraction of coronary arteries in coronary computed tomographic angiography. *Int J Cardiovasc Imag*, 28(4):921-933.
<https://doi.org/10.1007/s10554-011-9894-2>
- Yang JZ, Ma S, Sun Q, et al., 2014. Improved Hessian multiscale enhancement filter. *Biomed Mater Eng*, 24(6): 3267-3275. <https://doi.org/10.3233/BME-141149>
- Yang X, Cheng KTT, Chien A, 2014. Accurate vessel segmentation with progressive contrast enhancement and Canny refinement. *Asian Conf on Computer Vision*, p.1-16. https://doi.org/10.1007/978-3-319-16811-1_1
- Zhao SF, Zhou MQ, Jia TR, et al., 2014. Multi-branched cerebrovascular segmentation based on phase-field and likelihood model. *Comput Graph*, 38:239-247.
<https://doi.org/10.1016/j.cag.2013.11.004>